Eur. Phys. J. D **36**, 95–100 (2005)
DOI: 10.1140/epjd/e2005-00095-7

THE EUROPEAN PHYSICAL JOURNAL D

Collisions in a cesium hybrid optical and magnetic trap

N. Hoang[1], N. Zahzam[1], S. Guibal[2,a], and P. Pillet[1]

[1] Laboratoire Aimé Cotton, CNRS, Bâtiment 505, Campus d'Orsay, 91405 Orsay, France
[2] Laboratoire Matériaux et Phénomènes Quantiques, UMR 7162, CNRS/Université Denis Diderot-Paris 7, Case 7021, 2 place Jussieu, 75251 Paris Cedex 05, France

Received 3 September 2004 / Received in final form 14 April 2005
Published online 14 June 2005 –

Abstract. A new scheme for trapping Cs atoms in a non dissipative trap has been developed. The trap involves both optical dipole forces and magnetic forces. This device is suitable for Cs atoms in the lowest energy Zeeman sublevel, thus avoiding the two-body inelastic collisions which prevented reaching Bose-Einstein condensation of Cs in purely magnetic traps. Furthermore, an additional magnetic field can be applied, allowing a fine tuning of the two-body elastic collision cross-section. We report on the experimental realization of such a trap and describe the characteristics of the trapped atomic sample. An analysis of the collisional regime is performed using measurements of the damping of the oscillatory modes of the trapped atom cloud.

PACS. 05.30.Jp Boson systems – 32.80.Pj Optical cooling of atoms; trapping

1 Introduction

Bose-Einstein condensation (BEC) in an atomic cesium gas has recently been achieved in an optical dipole trap [1,2]. This experiment also introduces new experimental schemes and procedures in order to reach BEC for cesium atoms. The first attempts to reach BEC of Cs [3], following the same experimental route as for Rb or Na atoms [4,5] trapped by purely magnetic forces, were unsuccessful. In these experiments, the atoms were prepared in a low field seeking Zeeman sublevel, the energy of which is increasing with the magnetic field. Thus this state is not the true ground state, and exo-energetic spin-flip collisions are allowed. The inelastic two-body collision cross-section for cesium atoms appeared to be large enough to induce a rapid loss of atoms during the evaporative cooling process, and prevented the experiments from reaching BEC [6]. In contrast, the use of traps relying on optical dipole forces allows the atoms to be trapped in the lowest energy level; this therefore avoids inelastic collision losses and heating while allowing efficient evaporative cooling, and may be very efficient because of the high elastic two-body cross-section. However at high density, three-body collisions can occur, inducing heating and losses [7]. The cesium scattering length exhibits a strong dependence on the magnetic field due to the existence of low-field Feshbach resonances [8]. In the Cs BEC experiment described in [1], the cold cesium atoms are optically trapped in the lowest energy state $F = m_F = 3$, and the scattering length is varied during the evaporative cooling procedure in order to limit the three-body collision rate. From these experiments, it appears that a set-up suitable for Cs BEC should trap the Cs atoms in the $F = m_F = 3$ Zeeman sublevel, and should provide a variable magnetic field in order to vary the scattering length so as to allow an efficient evaporative cooling mechanism to take place. In this paper we discuss a hybrid optical and magnetic trap (HOM trap) for cesium atoms in the true hyperfine ground state, the high field seeking Zeeman sublevel, $F = m_F = 3$. We describe the trap geometry and the calculated potential shape, and we report the experimental trapping of cesium atoms in such a trap. We have characterized the trapping capability of our set-up and we present quantitative measurements of the number of trapped atoms, the temperature, and the lifetime of the sample. We provide a direct measurement of the oscillation frequency of the atoms in the harmonic potential along the vertical direction, and we analyse the damping of a breathing oscillatory mode. From this analysis, we are able to determine the collisional regime in the trapped atomic sample and the conditions for increasing efficiently the phase-space density through forced evaporative cooling.

2 The trap characteristics

2.1 Principle of the trap

The trap described in this paper relies both on optical dipole forces and magnetic forces. The lowest energy cesium level, $F = m_F = 3$, is a high field seeking state

[a] e-mail: samuel.guibal@paris7.jussieu.fr

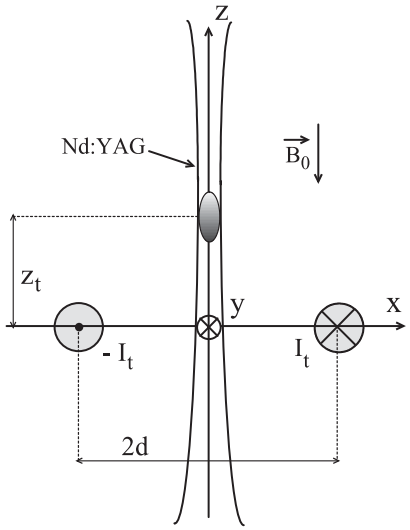

Fig. 1. The trap configuration in the (xz)-plane: $2d$ is the distance between the two bars, z_t is the trap height. The circles represent a pair of conductors each of which carries a total current I_t. The magnetic field gradient is chosen in order to compensate gravity at the trapping position ($\simeq$ 30 G/cm). The total magnetic field is adjustable between 20 and 80 G.

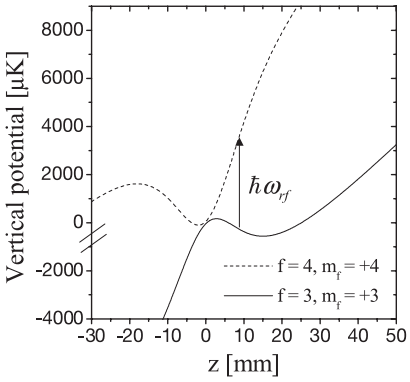

Fig. 2. Forced evaporative cooling scheme. A tunable microwave couples the magnetically trapped tate to the untrapped ones. The choice of the frequency of the applied microwave allows an energy elective evaporation.

which can not be confined in a purely magnetic potential (Maxwell's laws forbid the existence of a magnetic field maximum in all three directions). In our trapping scheme (see Fig. 1), one dimensional vertical magnetic confinement is created by a horizontal coil located below the desired trapping position. This magnetic field, combined with an oppositely directed variable homogeneous magnetic field leads to a confining magnetic potential along the vertical axis and a repulsive potential in the horizontal plane. A tight horizontal confinement is obtained using a vertically propagating, high power, far off resonance and red detuned laser beam. This scheme allows the implementation of one dimensional forced evaporative cooling by coupling the magnetically trapped state to an untrapped state via energy selective magnetic resonance in the microwave domain (Fig. 2). Although such one dimensional (1D) evaporative cooling is known to be less efficient than 2D or 3D, numerical simulations have shown that under proper conditions a large enough cooling rate can be achieved [9]. The trapping magnetic field is created by a horizontal coil located in the plane $z = 0$. In order to provide sufficient optical access, the coil is stretched along one direction so the field resembles that produced by a pair of wires. The coil dimensions are 10 cm along the y-axis and 2.5 cm along the x-axis, and its thickness is 8 mm. It is made of 50 windings of 1 mm diameter copper cable, and a typical current of 6 A is applied. A trapping position is found in the vicinity of the maximum value of the magnetic field located in the center of the coil. The trapping position moves to $z = 15$ mm when an oppositely directed homogeneous bias magnetic field B_0 is applied (for detailed calculation of the magnetic field and potentials, see Ref. [9]). A system of horizontal Helmholtz coils has been arranged in order to create this compensation field. This bias allows tuning of the value of the total magnetic field, with concomitant tuning of the scattering length a due to Feshbach resonances. Whereas the magnetic potential well can be as deep as 700 μK, the confinement remains weak: the oscillation frequency is about 4.6 Hz.

The optical dipole trap is formed by using a 15 W, 1064 nm Nd:YAG Gaussian laser beam. The frequency detuning from the closest cesium transition at 894.6 nm (D_1-Line) is $\delta = -1.2 \times 10^7 \Gamma$, where $\Gamma = 2\pi \times 4.56$ MHz is the full width at half maximum (FWHM) of the 894.6 nm transition. At this stage we neglect the spontaneous emission due to the excitation by the Nd:YAG laser. The beam waist of $w_0 = 260$ μm is chosen in order to maximize the number of atoms while keeping a reasonable trap depth $U_0 = 33$ μK. The Rayleigh length of the laser beam, equal to 20 cm, is large enough compared to the size of the atomic cloud to assume that the beam is parallel in the trapping area. The dipole trap radial frequency is $\omega_r/2\pi = 56$ Hz. The total potential has been plotted in Figure 3 in the vicinity of the trap centre. As shown, the vertical laser beam provides tight horizontal confinement, whereas the magnetic confinement along the vertical axis is weak. The potential exhibits a very anisotropic geometry leading to a cigar shape for the trapped atomic sample. For a temperature of 10 μK, the vertical dimension (RMS width) is expected to be 880 μm and the horizontal one 70 μm, assuming a thermal equilibrium.

2.2 Experimental set-up

The experimental arrangement consists of a two cell ultra-high vacuum set-up. These two cells are arranged vertically and separated by 58 cm. A magneto-optical trap (MOT) is operating in the upper one and is loaded from a low pressure thermal cesium vapour (10^{-9} mbar). A second MOT is located in the lower cell in which the residual pressure may be as low as 10^{-10} mbar due to a differential vacuum tube between the two cells. The first MOT acts as a cold atom source for the second one. The atoms are transfered via a free fall along the vacuum tube. The

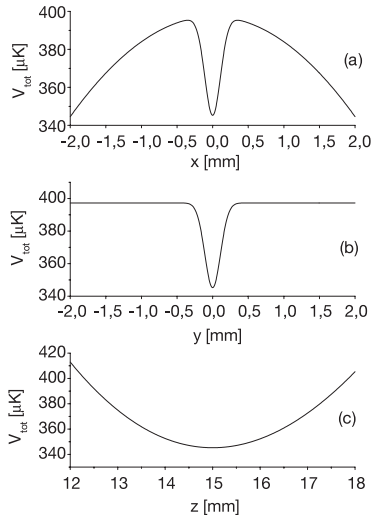

Fig. 3. The total potential $V_{tot}(x, y, z)$. (a) $V_{tot}(x, 0, z_t)$ versus x with $z_t = 15$ mm. There is a magnetic repulsion. The depth is around $k_B \times 50$ μK, $\omega_x/2\pi = 80$ Hz. (b) $V_{tot}(0, y, z_t)$ versus y. The depth is $k_B \times 50$ μK, $\omega_y/2\pi = 86$ Hz. (c) $V_{tot}(0, 0, z)$ versus z. The depth of the optical potential is $k_B \times 700$ μK, $\omega_z/2\pi = 4.5$ Hz.

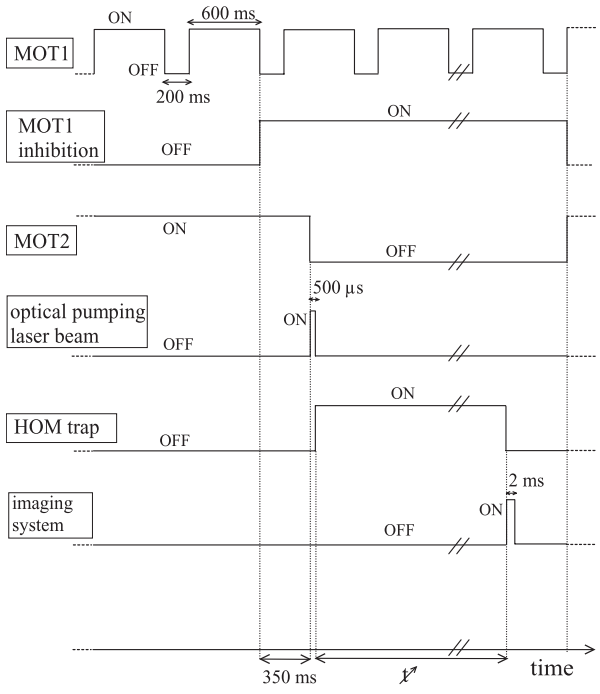

Fig. 4. A typical experimental sequence used for the loading of the hybrid trap.

center of the second MOT overlaps the trapping region of the HOM trap so that the atoms can be directly transfered from the MOT to the HOM trap. An imaging system based on a CCD camera provides the main diagnostics. A snap-shot of the atom sample can be recorded by applying a short (2 ms) resonant light pulse to the atoms. A typical experimental sequence is described Figure 4. The first MOT is loaded in about 1 second, 15 ms before releasing

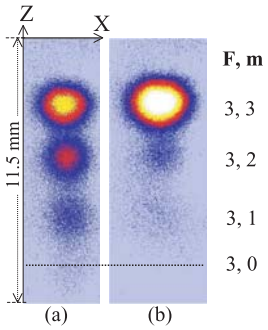

Fig. 5. Efficiency of the optical pumping into the $F = 3, m = 3$ state. The pictures are taken when a 70 G/cm vertical magnetic field gradient is applied during 30 ms; (a) without optical pumping, (b) with optical pumping. Only the atoms in the $F = 3, m = 3$ state can be trapped efficiently. A colour version of the figure is available in electronic format at `http://www.eurphysj.org`.

the atoms the beam detuning is increased from -3Γ to -10Γ (where $\Gamma \approx 5$ MHz is the natural linewidth of the cooling transition) and the magnetic field is switched-off. This optical molasses phase decreases the temperature below 10 μK. This is necessary to reduce the spreading of the atom cloud during the free fall to the second MOT and the attendant atom losses. Nearly 5% of the atoms reach the second MOT. Thus, this load/release operation is repeated (typically 6 times). At the end of this loading operation, the cloud is compressed by increasing the magnetic field gradient and the trapping beam detuning. Finally, the magnetic field is turned off, and a short optical molasses phase reduces the temperature below 7 μK. The goal of this compression and cooling phase is to provide a better matching of the atomic sample phase space volume to the characteristics (size and potential depth) of the HOM trap. After the MOT cut-off, a vertical homogeneous magnetic field (≈ 5 gauss) is applied in order to provide a quantization axis for the optical pumping of the atoms into the $F = 3, m = 3$ state. The optical pumping is performed using two laser beams tuned to the $F = 3, F' = 2$ transition for 300 μs. One σ^+ polarized beam propagates along the vertical axis. The second one is π polarized and propagates in the horizontal plane. This geometry allows a good optical pumping rate to the $F = 3, m = 3$ state. The atomic polarization efficiency can be measured by a longitudinal Stern-Gerlach separation. A vertical magnetic field gradient is applied during 30 ms and a picture is taken. The image (Fig. 5a) shows the separation into three clouds for which the magnetic force was opposite to gravity and which then remain in the imaging region. These clouds correspond to atoms into the $F = 3, m = 3, 2, 1$ states. When the optical pumping is applied, more than 90% of the atoms are found in the $F = 3, m = 3$ state (Fig. 5b). After the optical pumping phase, the trapping magnetic field is applied. After a variable evolution time in the HOM trap, the atoms are released and a picture is taken. This is the main diagnostic tool and the results of such an analysis are presented and discussed in the next part of the paper.

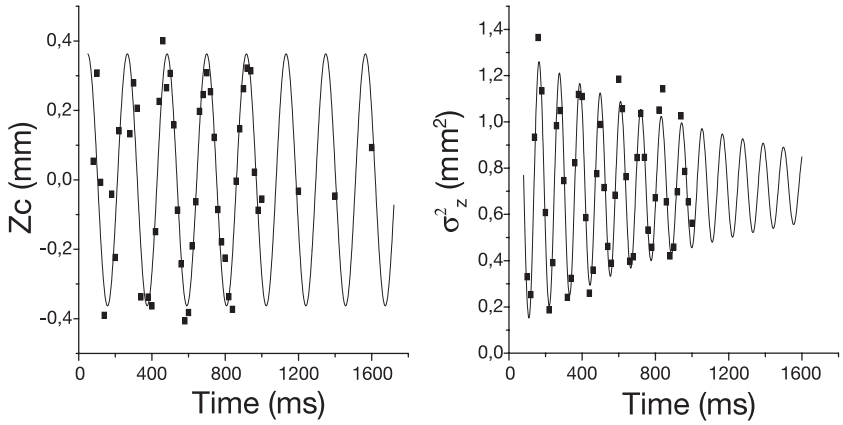

Fig. 6. Center-of-mass oscillations and rms width square oscillations along the vertical direction (Oz). The trap frequency ν_z, the oscillation frequency of the width ν_{σ_z} and its damping rate Γ given by the fit are respectively $\nu_z = 4.6(1)$ Hz, $\nu_{\sigma_z} = 9.11(2)$ Hz, $\Gamma/2\pi = 0.21(7)$ Hz.

3 Experimental measurements

3.1 Characteristics of the trapped atomic sample

About 15% of the atoms from the second MOT are transfered into the HOM trap, which leads typically to a few 10^6 atoms. The temperature is measured by time-of-flight experiments, and is found to be about $T = 5$ μK at this stage of experiment. This value is close to the temperature at the end of the molasses phase. The trap lifetime τ_{life} defined by $dN/dt = -N/\tau_{life}$ where N is the number of atoms in the trap, is also measured from the fluorescence signal decay versus time and is estimated to be around $\tau_{life} = 3.5$ s. Currently the trap lifetime is limited by the background pressure in the study cell. While the vacuum in the cell needs to be improved for an evaporative cooling process, it is adequate to characterize the collisional dynamics of the trapped atoms. The results of this study are presented in the next two sections.

3.2 Collective oscillations in the axial direction

Collective oscillations of the trapped cloud can be observed under the proper conditions. First, if the center of mass of the cloud is not at the center of the trap, then the cloud exhibits oscillatory center-of-mass motion. The center of the cloud oscillates as if it was a single particle in the trapping potential. This excitation is known as the dipole mode oscillation. This property makes observation of this mode a useful way of measuring trap frequencies. Secondly, it is typical that immediately after loading the trap the initial potential and kinetic energy of the trapped cloud are not in equilibrium. In this case, the width of the cloud will oscillate as the oscillations of the individual atoms convert potential to kinetic energy (and vice versa) once every quarter trap cycle. This oscillatory motion, known as the monopole-quadrupole mode, results from the coupling of the monopole mode and the quadrupole mode in an anisotropic trap. Calculations in references [10,11] based on the solution of the Boltzmann equation show that in an anisotropic trap the monopole-quadrupole mode exhibits damping. The damping is related to the elastic collisions. It gives some information about the collision rate in the trap and permits us to estimate the collision cross-section (such a study in cold metastable helium was demonstrated in [12]). In this approach we assume a pure harmonic trap, which is a reasonable approximation in our experiment since the temperature is at most as low as one sixth of the potential depth. In our trap, we observe and analyse these two collective classical motions of the trapped gas along the vertical direction. We focus our attention on oscillations along the vertical axis, as they have large amplitude compared to those along the horizontal directions[1]. We monitor, just after loading the trap, the evolution of the vertical position of the center-of-mass Z_c and the rms width squared along the z-axis σ_z^2. Figure 6 shows some typical measurements. The positions Z_c are fitted by a sine wave: $Z_c(t) = A + B\sin(2\pi\nu_z t + \varphi)$, from which we obtain the trap frequency ν_z. The squared width are fitted by an exponentially damped sine wave: $\sigma_z^2(t) = C + D\exp(-\Gamma t)\sin(2\pi\nu_{\sigma_z} t + \phi)$, from which we extract the oscillation frequency ν_{σ_z} and the damping rate Γ. For instance, the results in Figure 6, taken at $|B_0| \simeq 100$ G, give $\nu_z = 4.6(1)$ Hz, $\nu_{\sigma_z} = 9.11(2)$ Hz, $\Gamma/2\pi = 0.21(7)$ Hz. Taking into account the lifetime of the trap, the maximum loss of atoms during the damping time ($1/\Gamma = 0.8$ s) is about 20% (this effect is included in the error bars of Fig. 8). This experiment is repeated for different values of the magnetic bias $|B_0| = 60$ G, 70 G, 85 G, 100 G, 115 G, and 130 G. By changing the magnetic field value at the trapping position, we modify the scattering length a of the atoms via Feshbach resonances, which leads, for the above mentioned values of $|B_0|$, to $a = 300a_0$, $500a_0$, $700a_0$, $1000a_0$, $1200a_0$, $1400a_0$, respectively. For each value of $|B_0|$, we extract the ratios ν_{σ_z}/ν_z and $\Gamma/2\pi\nu_z$. The results are compared with the predictions of the classical theory of reference [10] for the case of a cigar-shaped trap (for which the anisotropy parameter $(\omega_z/\omega_r)^2 \ll 1$), as shown in Figure 7. One notes that the ratio ν_{σ_z}/ν_z decreases from 2 for the collisionless regime to 1.55 for the hydrodynamic regime, whereas $\Gamma/(2\pi\nu_z)$ goes to 0 at both ends but reaches a maximum between the two regimes. The results of Figure 7a and

[1] The amplitude of the oscillation scales as the trap frequency. The resolution of our detection apparatus is not high enough to allow a quantitative analysis of the radial motion.

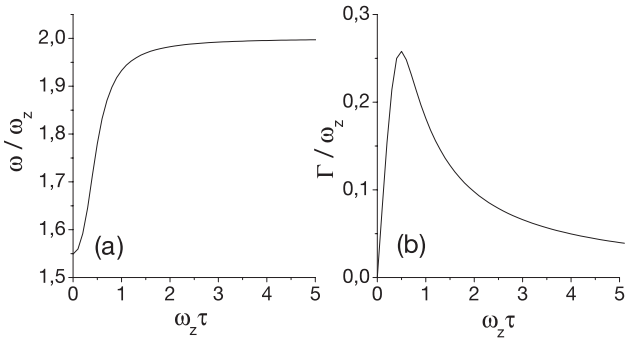

Fig. 7. Theoretical predictions issued from [10] for the lowest frequency "breathing" mode of a classical atomic cloud confined in a cigar-shaped trap, versus the elastic collision relaxation time. On part (a), plot of the oscillatory breathing mode pulsation ω, on part (b) plot of the oscillatory breathing mode damping rate Γ, both in units of ω_z, the axial (weak) trap pulsation.

Figure 7b can be combined to give the curve of Figure 8. The latter figure shows the experimental data we obtained superimposed to the theoretical predictions valid for a cigar-shaped trap. The comparison of our experimental data and the theoretical calculation allows us to make an indirect measurement of the elastic collision rate in the trapped cloud. As a comparison, we plotted the points calculated for a number of atoms $N = 1 \times 10^6$ (similar to the number of the atoms transferred into the trap), at different temperatures $T = 10\,\mu$K (symbol $\times$ in the figure), 5 μK (symbol $\star$), 1 μK (symbol $\circ$), and for different values of the scattering length $a = 300a_0$, $500a_0$, $700a_0$, $1000a_0$, $1200a_0$, $1400a_0$. For each calculated point, we evaluated the product $2\pi\nu_z \times \tau$, where the relaxation time $\tau \propto 1/\gamma_{coll}$, $\gamma_{coll} = \overline{n}\sigma\overline{v_r}$ being the classical collision rate ($\overline{n} = (1/\sqrt{8})N\omega_r^2\omega_z\,(m/2\pi k_B T)^{3/2}$ is the average density, $\overline{v_r} = 4\sqrt{k_B T/\pi m}$ is the mean relative velocity of the atoms, and $\sigma = \sigma(a,T) = \langle 8\pi a^2/(1+k^2a^2)\rangle_T$ is the thermal average of the elastic collision cross-section).

3.3 Discussion

First, we notice from the position of the experimental data on the curve in Figure 8 that the collision rate in the trapped cloud is relatively low. This low collision rate results from a low spatial density. At this stage of the experiment, no forced evaporative cooling has been performed and the temperature of 5 μK prevents us from reaching high densities. In addition, the loading efficiency from the MOT2 to the trap of about 15% is not sufficient to provide a high atomic number, and thus high densities in the trap.

Second, we observe that the increase of the scattering length value from $300a_0$ to $1000a_0$ is not sufficient to increase drastically the collision rate in the experiment. Therefore it seems that at the temperature currently reached in the experiment, the elastic collision cross-section depends only slightly on the scattering length. Under such conditions, the elastic collision cross-section is governed by the temperature, suggesting a regime near the unitary limit ($ka \gg 1$) where $\sigma = 8\pi/k^2$. Hence, in this regime, the relaxation time $\tau \propto 1/\overline{n}\sigma\overline{v_r}$ scales as $1/(NT^{-3/2})T^{-1}T^{1/2} = T^2/N$.

All the above mentioned conclusions are similar for the calculated points corresponding to an atomic cloud of $N = 1 \times 10^6$ atoms at the temperatures of 10 μK and 5 μK. In both cases, the collisional regime remains in the vicinity of the collisionless regime $2\pi\nu_z \times \tau \to \infty$ and both temperatures are not low enough to allow an increase of the elastic collision cross-section by increasing the scattering length from $300a_0$ to $1400a_0$.

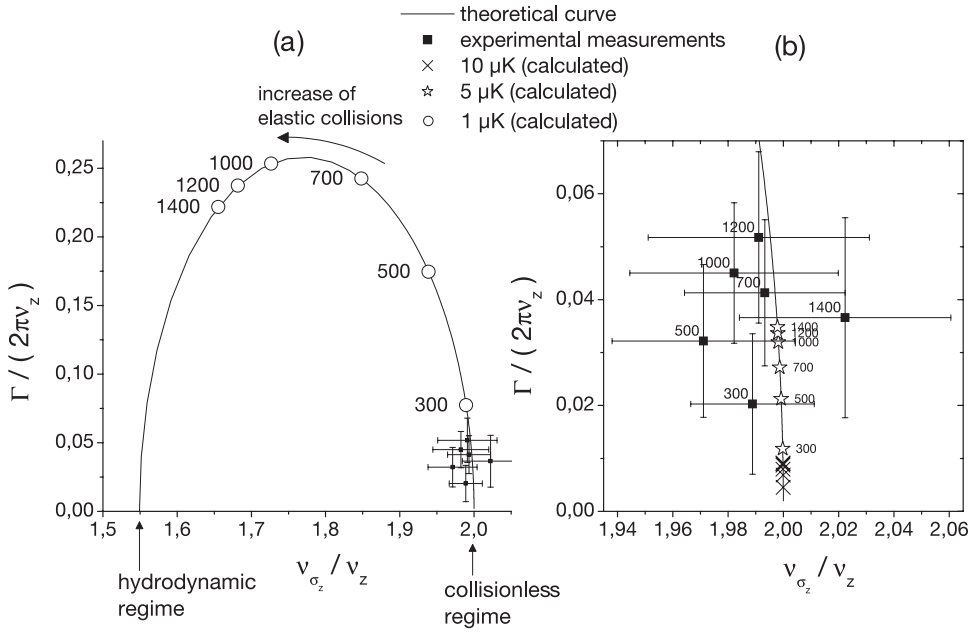

Fig. 8. Plot of the frequencies ν_{σ_z} and damping rates Γ of the lowest "breathing" mode. The arrow indicates the displacement on the curve when the elastic collision rate increases. Experimental measurements (■) are reported on part (a) and (b) (zoom in of the (a) part)) as a function of the scattering length (value indicated in labels). As a comparison we report some calculations performed for an atomic cloud of $N = 1 \times 10^6$ atoms at the temperature of $T = 10$ μK ($\times$), $T = 5$ μK ($\star$), and $T = 1$ μK ($\circ$), versus the scattering length (labels).

However, an atomic cloud of $N = 1 \times 10^6$ atoms at the temperature of 1 μK exhibits different collisional dynamics. The temperature is sufficiently low to allow control of the elastic collision rate by tuning the scattering length. Indeed, Figure 8 shows that the increase of the scattering length from $300a_0$ to $1400a_0$ allows a collisional regime halfway between the collisionless one and the hydrodynamic one $2\pi\nu_z \times \tau \rightarrow 0$. We note that the scattering length value near $1000a_0$ corresponds to the top of the curve in Figure 8, that is at the maximum of the damping rate Γ. Such a collisional regime (halfway between the collisionless and hydrodynamic regimes) is of interest in the evaporative cooling process, as its corresponding elastic collision rate is relatively high, without reaching the hydrodynamic regime (such a regime is to be avoided during the evaporative process). Thus it is worth estimating how much the elastic collision rate needs to be increased in our experiment in order to reach the top of the curve in Figure 8. Figure 7b shows that the maximum for Γ is reached for $2\pi\nu_z \times \tau \simeq 0.5$. In Figure 8, the experimental points are in the vicinity of the calculated points corresponding to $N = 1 \times 10^6$ atoms and a temperature $T = 5$ μK. Therefore, the value of the product $2\pi\nu_z \times \tau$ is expected to be the same for these two groups of points. For an atomic cloud of $N = 1 \times 10^6$ atoms at the temperature of $T = 5$ μK, thus for the experimental points, the product $2\pi\nu_z \times \tau$ is estimated to 4. It means that in the experiment, the relaxation time τ and thus the rate T^2/N needs to be decreased by a factor of 8, in order to reach a collisional regime favourable to efficient evaporative cooling.

4 Conclusion

In this paper we have described a hybrid optical and magnetic trap (HOM trap) for cesium atoms that confines high-field seeking states near a maximum of the magnetic field, and analyzed the trap to assess its suitability to achieve BEC. The trap is not subject to Majorana spin flips and therefore turns off the two particle inelastic processes that have prevented previous attempts to reach Bose-Einstein condensation in cesium in pure magnetic traps. We also report on the experimental observation of the trapping capability of our set-up, and on its characterization through fluorescence imaging and a powerful measurement method (based on the study of the collective excitation modes of the atomic cloud) to characterize the collisional regime in the HOM trap. In particular, we demonstrated a low collisional regime, near the collisionless one, from the analysis of collective oscillations versus the scattering length. At this stage of the experiment, the increase of the scattering length from $300a_0$ to $1400a_0$ does not allow usto reach a sufficiently high collisional regime to proceed to BEC. The relatively high temperature $T = 5$ μK prevents us from reaching a regime where the elastic collision cross-section depends on the scattering length. Furthermore, the number of trapped atoms has to be increased to provide a higher spatial density. In order to improve the loading of the HOM trap, we could apply a sideband cooling method, which can effectively be performed in optical lattices [13,14]. Such a method can reach temperatures of a few microkelvins with spatial densities of the order of 10^{12} atoms/cm^3, which is a good starting point for the evaporative cooling process. Numerical simulations of the evaporative cooling in the trap were reported in a previous paper [9] and have demonstrated that BEC could be reached within a reasonable time in such a trap. The experimental route towards BEC has been demonstrated by the Innsbruck group [1] and a similar approach could be implemented in our set-up.

This work is supported by "Action Concertée Incitative Photonique" of the French research Ministry. The people involved in this work are members of the European Network "Cold Molecules" NHPRN-CT-2002-00290. The authors thank Salah Boussen, Daniel Comparat, Jacques Pinard, Laurence Pruvost, and Nicolas Vanhaecke for fruitful discussion.

References

1. T. Weber, J. Herbig, M. Mark, H.-C. Nägerl, R. Grimm, Science **299**, 232 (2003)
2. D. Rychtarik, B. Engeser, H.-C. Nägerl, R. Grimm, Phys. Rev. Lett. **92**, 173003 (2004).
3. J. Söding, D. Guéry-Odelin, P. Desbiolles, G. Ferrari, J. Dalibard, Phys. Rev. Lett. **80**, 1869 (1998)
4. M.H. Anderson, J.R. Ensher, M.R. Matthews, C.E. Wieman, E.A. Cornell, Science **269**, 198 (1995)
5. K.B. Davis, M.-O. Mewes, M.R. Andrews, N.J. van Druten, D.S. Durfee, D.M. Kurn, W. Ketterle, Phys. Rev. Lett. **75**, 3969 (1995)
6. D. Guéry-Odelin, J. Söding, P. Desbiolles, Jean Dalibard, Europhys. Lett. **44**, 26 (1998)
7. T. Weber, J. Herbig, M. Mark, H.-C. Nägerl, R. Grimm, Phys. Rev. Lett. **91**, 123201–1 (2003)
8. A.J. Kerman, C. Chin, V. Vuletić, S. Chu, P.J. Leo, C.J. Williams, P.S. Julienne, C.R. Acad. Sci Paris **t.2**, 633 (2001)
9. S. Boussen, N. Hoang, S. Guibal, N. Zahzam, L. Pruvost, D. Marescaux, J. Pinard, P. Pillet, Eur. Phys. J. D **28**, 259 (2004)
10. D. Guéry-Odelin, F. Zambelli, J. Dalibard, S. Stringari, Phys. Rev. A **60**, 4851 (1999)
11. U. Al Khawaja, C.J. Pethick, H. Smith, J. Low Temp. Phys. **118**, 127 (2000)
12. M. Leduc, J. Léonard, F. Pereira Dos Santos, E. Jahier, S. Schwartz, C. Cohen-Tannoudji, Phys. Acta Pol. B **33**, 2213 (2002)
13. D.J. Han, S. Wolf, S. Oliver, C. McCormick, M.T. DePue, D.S. Weiss, Phys. Rev. Lett. **85**, 724 (2000)
14. D.J. Han, M.T. DePue, D.S. Weiss, Phys. Rev. A **63**, 023405–1 (2001)